An accurate and highly efficient three-dimensional tidal model and its application to Dalian Bay

Ruijin ZHANG*, Zhaochen SUN**, Norio HAYAKAWA***, Tokuzo HOSOYAMADA***

An accurate and highly efficient semi-implicit three-dimensional tidal model is developed and applied to Dalian Bay. In the model, the pressure gradient in the momentum equations and the velocities in the vertically integrated continuity equation are discretized using the θ-method, the θ representing an implicit parameter. At each time step the numerical method requires the solution of one large linear system which can be formally decomposed into a set of small three-diagonal systems coupled with one five-diagonal system. The algorithm has been shown to be fast and accurate. The 3-D model is first tested against an analytical solution for the simple case of rectangular basins. The computed velocity and free surface water elevation results coincide with the analytical results. The model is next applied to Dalian Bay. The predicted results show good agreement with field measurement, verifying the accuracy of the model.

Key words : three-dimensional model; semi-implicit; Dalian Bay

1. Introduction

Accurate prediction of the tidal flow in offshore and coastal waters is the basis for offshore, coastal engineering and ocean environmental studies. Numerical simulation of tidal flow in coastal areas is widely used in these fields. Several numerical methods for the time-dependent two- and three-dimensional equations for the tidal motion are reported in the recent scientific papers[1,2,3], and are now implemented in practical applications. The time integration schemes of these methods range from fully explicit to fully implicit. A fully explicit finite difference method is relatively simple to implement and is easily vectorizable. However, a severe limitation exists for the standard explicit numerical methods owing to the propagation of surface gravity waves, known as the Courant-Friedrich-Lewy (CFL) stability criterion. Several existing numerical models for two- and three-dimensional shallow water flow simulations are based on an alternative direction implicit (ADI) method. ADI methods have superior computational efficiency compared to fully explicit methods because their improved stability allows for the introduction of a larger time step. However, the so-called ADI effect[4], which is a source of inaccuracy, arises when these methods are used with a large time step in flow domains characterized by complex geometries. And ADI method is primarily applied to two-dimensional calculations because of its complicated nature of the numerical algorithm. To overcome these obstacles of the traditional numerical methods, Casulli[5,6] introduced a fast and accurate semi-implicit method to calculate tidal waves. In this paper, the algorithm developed by Casulli is explained briefly and numerical experiment is performed to verify its accuracy and efficiency. The model is then applied to Dalian Bay for further verification. This application studies the hydrodynamic conditions, such as the instantaneous current vectors and the tidal residual current, of Dalian Bay.

received May 16, 2003

*Graduate School, Nagaoka Univ. of Tech
**State Key Lab. of Coastal and Offshore Eng.,Dalian Univ. of Tech
***Dept. of Civil and Environment Eng., Nagaoka Univ. of Tech

2. Model Description

This model is a semi-implicit three-dimensional tidal model. Tidal currents are calculated using the equations for the tidal motion with the Coriolis force. The calculation domain is three-dimensional.

2.1 Governing Equations

The governing three-dimensional, primitive variable equations describing constant density free surface flows in estuarine embayment and coastal seas have been derived from the Navier-Stokes equations under the simplifying assumption that the pressure is hydrostatic. Such equations have the following form:

$$\frac{\partial u}{\partial t}+u\frac{\partial u}{\partial x}+v\frac{\partial u}{\partial y}+w\frac{\partial u}{\partial z}= -g\frac{\partial \eta}{\partial x}+\mu_H\left(\frac{\partial^2 u}{\partial x^2}+\frac{\partial^2 u}{\partial y^2}\right)+\frac{\partial}{\partial z}\left(\mu_V\frac{\partial u}{\partial z}\right)+fv \quad (1)$$

$$\frac{\partial v}{\partial t}+u\frac{\partial v}{\partial x}+v\frac{\partial v}{\partial y}+w\frac{\partial v}{\partial z}= -g\frac{\partial \eta}{\partial y}+\mu_H\left(\frac{\partial^2 v}{\partial x^2}+\frac{\partial^2 v}{\partial y^2}\right)+\frac{\partial}{\partial z}\left(\mu_V\frac{\partial v}{\partial z}\right)-fu \quad (2)$$

$$\frac{\partial u}{\partial x}+\frac{\partial v}{\partial y}+\frac{\partial w}{\partial z}=0 \quad (3)$$

where $u(x, y, z, t)$, $v(x, y, z, t)$ and $w(x, y, z, t)$ are the velocity components in the horizontal x and y- directions and in the vertical z-direction, respectively. t is time, $\eta(x, y, t)$ is the water surface elevation measured from the height of the undisturbed water surface, g is the gravitational acceleration, f is the Coriolis parameter, which is assumed to be constant, and μ_H and μ_V are the horizontal and vertical eddy viscosity coefficients, respectively.

The following free surface equation is generated by integrating the continuity equation over the depth and using the kinematic condition at the free surface.

$$\frac{\partial \eta}{\partial t}+\frac{\partial}{\partial x}\left[\int_h^\eta u dz\right]+\frac{\partial}{\partial y}\left[\int_h^\eta v dz\right]=0 \quad (4)$$

In this equation, $h(x, y, t)$ is the water depth measured from the undisturbed water surface. The total water depth $H(x, y, t)$ is given by

$$H(x,y,t)=h(x,y,t)+\eta(x,y,t) \quad (5)$$

$\eta(x, y, t)$ is defined above.

2.2 Boundary Conditions

The boundary conditions at the free surface are specified by the prescribed wind stress:

$$\mu_V\frac{\partial u}{\partial z}=\frac{\tau_x^w}{\rho},\quad \mu_V\frac{\partial v}{\partial z}=\frac{\tau_y^w}{\rho}. \quad (6)$$

where τ_x^w and τ_y^w are the shear stress at the water surface in the x and y direction.

The boundary conditions at the sediment-water interface are related to the bottom stress, which is specified by the Manning-Chezy formula:

$$\mu_V\frac{\partial v}{\partial z}=\gamma v,\quad \mu_V\frac{\partial u}{\partial z}=\gamma u, \quad (7)$$

where $\gamma=g\frac{\sqrt{u^2+v^2}}{c_z^2}$ and C_z is the Chezy coefficient.

2.3 Numerical Scheme

The governing equations with their boundary conditions are solved using the finite difference technique. A staggered arrangement of grid points is used, as depicted in Fig. 1.

Equations (8) and (9) show the discretization of the horizontal momentum governing Equations (1) and (2), respectively. The term F on the right side of Equation (8) corresponds to terms that are associated with $u^n_{i+\frac{1}{2},j,k}$, which are explicit terms. The remaining terms on the right side of the equation are the surface gradient and the vertical convection term, which are treated semi-implicitly. In case of ADI method, implicit treatment for the horizontal momentum equation is restricted only to horizontal momentum. Whereas in this scheme, implicit treatment is applied not only to the horizontal velocity but also to the surface gradient. The symbol θ is a mixing coefficient expressing the degree of implicit and explicit treatment.

$$u^{n+1}_{i+\frac{1}{2},j,k}=Fu^n_{i+\frac{1}{2},j,k} -g\frac{\Delta t}{\Delta x}\left[\theta\left(\eta^{n+1}_{i+1,j}-\eta^{n+1}_{i,j}\right)+(1-\theta)\left(\eta^n_{i+1,j}-\eta^n_{i,j}\right)\right]+\Delta t\times \frac{\mu_{V\,k+\frac{1}{2}}\dfrac{u^{n+1}_{i+\frac{1}{2},j,k+1}-u^{n+1}_{i+\frac{1}{2},j,k}}{\Delta z_{i+\frac{1}{2},j,k+\frac{1}{2}}}-\mu_{V\,k-\frac{1}{2}}\dfrac{u^{n+1}_{i+\frac{1}{2},j,k}-u^{n+1}_{i+\frac{1}{2},j,k-1}}{\Delta z_{i+\frac{1}{2},j,k-\frac{1}{2}}}}{\Delta z_{i+\frac{1}{2},j,k}} \quad (8)$$

$$v^{n+1}_{i,j+\frac{1}{2},k}=Fv^n_{i,j+\frac{1}{2},k} -g\frac{\Delta t}{\Delta y}\left[\theta\left(\eta^{n+1}_{i,j+1},-\eta^{n+1}_{i,j}\right)+(1-\theta)\left(\eta^n_{i,j+1}-\eta^n_{i,j}\right)\right]+\Delta t\times \frac{\mu_{V\,k+\frac{1}{2}}\dfrac{v^{n+1}_{i,j+\frac{1}{2},k+1}-v^{n+1}_{i,j+\frac{1}{2},k}}{\Delta z_{i,j+\frac{1}{2},k+1}}-\mu_{V\,k-\frac{1}{2}}\dfrac{v^{n+1}_{i,j+\frac{1}{2},k}-v^{n+1}_{i,j+\frac{1}{2},k-1}}{\Delta z_{i,j+\frac{1}{2},k-\frac{1}{2}}}}{\Delta z_{i,j+\frac{1}{2},k}} \quad (9)$$

Let m and M denote the k-index of the bottom and of the top finite difference stencil respectively. Both m and M

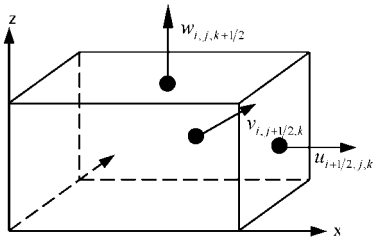

Fig. 1 Variable configuration

vary with the spatial position and the value of M varies also with time. For notational simplicity, however, these indices will be omitted. Using this notation, the boundary conditions at the free surface and at the sediment-water interface, (6) and (7), are written in difference form as

$$\nu_{i+\frac{1}{2},j,M+\frac{1}{2}}\frac{u^{n+1}_{i+\frac{1}{2},j,M+1}-u^{n+1}_{i+\frac{1}{2},j,M}}{\Delta z_{i+\frac{1}{2},j,M+\frac{1}{2}}}=\tau^{w}_{x} \tag{10}$$

$$\nu_{i,j+\frac{1}{2},M+\frac{1}{2}}\frac{v^{n+1}_{i,j+\frac{1}{2},M+1}-v^{n+1}_{i,j+\frac{1}{2},M}}{\Delta z_{i,j+\frac{1}{2},M+\frac{1}{2}}}=\tau^{w}_{y} \tag{11}$$

$$\nu_{i+\frac{1}{2},j,m-\frac{1}{2}}\frac{u^{n+1}_{i+\frac{1}{2},j,m}-u^{n+1}_{i+\frac{1}{2},j,m-1}}{\Delta z_{i+\frac{1}{2},j,m-\frac{1}{2}}}=\gamma^{n+\frac{1}{2}}_{i+\frac{1}{2},j,m}u^{n+1}_{i+\frac{1}{2},j,m} \tag{12}$$

$$\nu_{i,j+\frac{1}{2},m-\frac{1}{2}}\frac{v^{n+1}_{i,j+\frac{1}{2},m}-v^{n+1}_{i,j+\frac{1}{2},m-1}}{\Delta z_{i,j+\frac{1}{2},m-\frac{1}{2}}}=\gamma^{n+\frac{1}{2}}_{i,j+\frac{1}{2},m}u^{n+1}_{i,j+\frac{1}{2},m} \tag{13}$$

Equation (4) is discretized into Equation (10). All terms are treated implicitly with a mixing coefficient θ.

$$\begin{aligned}\eta^{n+1}_{i,j}&=\eta^{n}_{i,j}\\&-\frac{\Delta t}{\Delta x}\theta\left[\sum_{k=m}^{M}\Delta z_{i+\frac{1}{2},j,k}u^{n+1}_{i+\frac{1}{2},j,k}-\sum_{k=m}^{M}\Delta z_{i-\frac{1}{2},j,k}u^{n+1}_{i-\frac{1}{2},j,k}\right]\\&-\frac{\Delta t}{\Delta y}\theta\left[\sum_{k=m}^{M}\Delta z_{i,j+\frac{1}{2},k}v^{n+1}_{i,j+\frac{1}{2},k}-\sum_{k=m}^{M}\Delta z_{i,j-\frac{1}{2},k}v^{n+1}_{i,j-\frac{1}{2},k}\right]\\&-\frac{\Delta t}{\Delta x}(1-\theta)\left[\sum_{k=m}^{M}\Delta z_{i+\frac{1}{2},j,k}u^{n}_{i+\frac{1}{2},j,k}-\sum_{k=m}^{M}\Delta z_{i-\frac{1}{2},j,k}u^{n}_{i-\frac{1}{2},j,k}\right]\\&-\frac{\Delta t}{\Delta y}(1-\theta)\left[\sum_{k=m}^{M}\Delta z_{i,j+\frac{1}{2},k}v^{n}_{i,j+\frac{1}{2},k}-\sum_{k=m}^{M}\Delta z_{i,j-\frac{1}{2},k}v^{n}_{i,j-\frac{1}{2},k}\right]\end{aligned} \tag{14}$$

2.4 Euler-Lagrangian Discretization of Convective and Viscous Terms

In the discretized momentum equations, Equation (8) and (9), the explicit terms Fu, Fv consist of both convection and horizontal viscous terms. The discretization of convective and viscous terms causes one of the major difficulties in the numerical treatment of the equations for the tidal motion. Equation (15), provides an example of the advection-diffusion of c:

$$\frac{\partial c}{\partial t}+u\frac{\partial c}{\partial x}+v\frac{\partial c}{\partial y}+w\frac{\partial c}{\partial z}=\mu_H\left(\frac{\partial^2 c}{\partial x^2}+\frac{\partial^2 c}{\partial y^2}\right)+\frac{\partial}{\partial z}\left(\mu_V\frac{\partial c}{\partial z}\right) \tag{15}$$

here μ_H and μ_V are non-negative diffusion coefficients. The symbol c denotes either u or v.

In order to improve the stability and accuracy of an explicit finite difference method, Equation (15) is written in the Lagrangian form

$$\frac{dc}{dt}=\mu_H\left(\frac{\partial^2 c}{\partial x^2}+\frac{\partial^2 c}{\partial y^2}\right)+\frac{\partial}{\partial z}\left(\mu_V\frac{\partial c}{\partial z}\right) \tag{16}$$

where the substantial derivative d/dt indicates the time rate of change. This value is calculated along the streak line defined by

$$\frac{dx}{dt}=u,\quad \frac{dy}{dt}=v,\quad \frac{dz}{dt}=w \tag{17}$$

The natural semi-implicit discretization of Equation (15) is calculated as

$$\begin{aligned}&\frac{c^{n+1}_{i,j,k}-c^{n}_{i-a,j-b,k-d}}{\Delta t}=\\&\frac{\mu_{V\,k+1/2}\dfrac{c^{n+1}_{i,j,k+1}-c^{n+1}_{i,j,k}}{\Delta z_{i,j,k+1/2}}-\mu_{V\,k-1/2}\dfrac{c^{n+1}_{i,j,k}-c^{n+1}_{i,j,k-1}}{\Delta z_{i,j,k-1/2}}}{\Delta z_{i,j,k}}\\&+\mu_H\left(\frac{c^{n}_{i-a+1,j-b,k-d}-2c^{n}_{i-a,j-b,k-d}+c^{n}_{i-a-1,j-b,k-d}}{\Delta x^2}\right.\\&\left.+\frac{c^{n}_{i-a,j-b+1,k-d}-2c^{n}_{i-a,j-b,k-d}+c^{n}_{i-a,j-b-1,k-d}}{\Delta y^2}\right)\end{aligned} \tag{18}$$

where $a=u\Delta t/\Delta x$, $b=v\Delta t/\Delta y$, $d=w\Delta t/\Delta z$ are the grid Courant number.

It is important to understand the physical significance of Equation (18). The values of c at and around (i, j, k) at time t_{n+1} are related to the c-values at and around $(i\text{-}a, j\text{-}b, k\text{-}d)$ at time t_n. Moreover $(i\text{-}a, j\text{-}b, k\text{-}d)$ denotes a point on the same streak line that passes through (i, j, k) at time t_{n+1}. Thus Equation (14) is not just a simple algorithm, but it is also capable of correctly accounting for both convection and diffusion. In general, a, b and d are not integers, therefore $(i\text{-}a,j\text{-}b,k\text{-}d)$ is not a grid point. An interpolation formula must then be used to define $c^{n}_{i-a,j-b,k-d}$.

The chosen interpolation formula affects the accuracy, stability, numerical diffusion and spurious oscillations of Equation (18). The interpolation used for calculating $c^{n}_{i-a,j-b,k-d}$ is a tri-linear interpolation over the eight surrounding mesh points. For a positive a, b and d, let l, m, n be the integer parts of a, b and d, respectively, and p, q and r be their corresponding decimal parts, so that $a=l+p$, $b=m+q$ and $d=n+r$. Then $c^{n}_{i-a,j-b,k-d}$ is approximated by

$$
\begin{aligned}
&c^n_{i-a,j-b,k-d} = \\
&(1-r)\{(1-p)[(1-q)c^n_{i-l,j-m,k-n}+qc^n_{i-l,j-m-1,k-n}] \\
&\quad + p[(1-q)c^n_{i-l-1,j-m,k-n}+qc^n_{i-l-1,j-m-1,k-n}]\} \\
&\quad + r\{(1-p)[(1-q)c^n_{i-1,j-m,k-n-1}+qc^n_{i-l,j-m-1,k-n-1}] \\
&\quad + p[(1-q)c^n_{i-l-1,j-m,k-n-1}+qc^n_{i-l-1,j-m-1,k-n-1}]\}
\end{aligned} \tag{19}
$$

After this approximation, the Euler-Lagrangian method can easily be used to discretize the convective and viscous terms in momentum Equations（2）and（3）. The finite difference operator F in Equations（8）and（9）is defined in Equations（20）and（21）.

$$
\begin{aligned}
&Fu^{n+1}_{i+1/2,j,k} = u^n_{i-1/2-a,j-b,k-d} \\
&+\mu_H\Delta t\left(\frac{u^n_{i-1/2-a+1,j-b,k-d}-2u^n_{i+1/2-a,j-b,k-d}+u^n_{i+1/2-a-1,j-b,k-d}}{\Delta x^2}\right. \\
&\left.+\frac{u^n_{i+1/2-a,j-b-1,k-d}-2u^n_{i+1/2-a,j-b,k-d}+u^n_{i+1/2-a,j-b-1,k-d}}{\Delta y^2}\right) \\
&+f\Delta t v^n_{i-1/2-a,j-b,k-d}
\end{aligned} \tag{20}
$$

$$
\begin{aligned}
&Fv^{n+1}_{i,j+1/2,k} = v^n_{i-a,j+1/2-b,k-d} \\
&+\mu_H\Delta t\left(\frac{v^n_{i-a+1,j+1/2-b,k-d}-2v^n_{i-a,j+1/2-b,k-d}+v^n_{i-a-1,j+1/2-b,k-d}}{\Delta x^2}\right. \\
&\left.+\frac{v^n_{i-a,j+1/2-b+1,k-d}-2v^n_{i-a,j+1/2-b,k-d}+v^n_{i-a,j+1/2-b-1,k-d}}{\Delta y^2}\right) \\
&+f\Delta t u^n_{i-a,j+1/2-b,k-d}
\end{aligned} \tag{21}
$$

2.5 Solution Algorithm

The numbers of the unknowns for the governing equation of both u and v are $N_xN_yN_z$, and that for η, is N_xN_y. Therefore, the linear system consists of N_xN_y（$2N_z+1$）discretized governing equations. Since a linear system containing N_xN_y（$2N_z+1$）equations can become quite large, even for modest values of N_xN_y and N_z, the system of Equations（8）～(10) is first decomposed into a set of $2N_xN_y$ independent tridiagonal systems of N_z equations, and one five-diagonal system of N_xN_y equations. Specifically, Equations（8）～(10) are first written in the matrix form as

$$
A^n_{i+\frac{1}{2},j}U^{n+1}_{i+\frac{1}{2},j} = G^n_{i+\frac{1}{2},j} - g\frac{\Delta t}{\Delta x}\left[\theta\left(\eta^{n+1}_{i+1,j}-\eta^{n+1}_{i,j}\right)\right]\Delta Z^n_{i+\frac{1}{2},j} \tag{22}
$$

$$
A^n_{i,j+\frac{1}{2}}V^{n+1}_{i,j+\frac{1}{2}} = G^n_{i,j+\frac{1}{2}} - g\frac{\Delta t}{\Delta y}\left[\theta\left(\eta^{n+1}_{i,j+1}-\eta^{n+1}_{i,j}\right)\right]\Delta Z^n_{i,j+\frac{1}{2}} \tag{23}
$$

$$
\begin{aligned}
\eta^{n+1}_{i,j} &= \delta^n_{i,j} \\
&-\frac{\Delta t}{\Delta x}\theta\left[\left(\Delta Z^n_{i+\frac{1}{2},j}\right)^T U^{n+1}_{i+\frac{1}{2},j}-\left(\Delta Z^n_{i-\frac{1}{2},j}\right)^T U^{n+1}_{i-\frac{1}{2},j}\right] \\
&-\frac{\Delta t}{\Delta y}\theta\left[\left(\Delta Z^n_{i,j+\frac{1}{2}}\right)^T V^{n+1}_{i,j+\frac{1}{2}}-\left(\Delta Z^n_{i,j-\frac{1}{2}}\right)^T V^{n+1}_{i,j-\frac{1}{2}}\right]
\end{aligned} \tag{24}
$$

The vertical vectors U, V, G and ΔZ represent the u, v, in explicit terms and Δz at each vertical layer.

$$
G^n_{i+\frac{1}{2},j} = \begin{pmatrix}
\Delta z_M\left[Fu^n_{i+\frac{1}{2},j,M}-g\frac{\Delta t}{\Delta x}(1-\theta)*\left(\eta^n_{i+1,j}-\eta^n_{i,j}\right)\right] \\
+\Delta t\tau^w_x \\
\Delta z_{M-1}\left[Fu^n_{i+\frac{1}{2},j,M-1}-g\frac{\Delta t}{\Delta x}(1-\theta)*\left(\eta^n_{i+1,j}-\eta^n_{i,j}\right)\right] \\
\vdots \\
\Delta z_{m+1}\left[Fu^n_{i+\frac{1}{2},j,m+1}-g\frac{\Delta t}{\Delta x}(1-\theta)*\left(\eta^n_{i+1,j}-\eta^n_{i,j}\right)\right] \\
\Delta z_m\left[Fu^n_{i+\frac{1}{2},j,m}-g\frac{\Delta t}{\Delta x}(1-\theta)*\left(\eta^n_{i+1,j}-\eta^n_{i,j}\right)\right]
\end{pmatrix} \tag{25}
$$

$$
U^{n+1}_{i+\frac{1}{2},j} = \begin{pmatrix}
u^{n+1}_{i+\frac{1}{2},j,M} \\
u^{n+1}_{i+\frac{1}{2},j,M-1} \\
\vdots \\
u^{n+1}_{i+\frac{1}{2},j,m+1} \\
u^{n+1}_{i+\frac{1}{2},j,m}
\end{pmatrix} \tag{26}
\qquad
V^{n+1}_{i,j+\frac{1}{2}} = \begin{pmatrix}
v^{n+1}_{i,j+\frac{1}{2},M} \\
v^{n+1}_{i,j+\frac{1}{2},M-1} \\
\vdots \\
v^{n+1}_{i,j+\frac{1}{2},m+1} \\
v^{n+1}_{i,j+\frac{1}{2},m}
\end{pmatrix} \tag{27}
$$

$$
G^n_{i,j+\frac{1}{2}} = \begin{pmatrix}
\Delta z_M\left[Fv^n_{i,j+\frac{1}{2},M}-g\frac{\Delta t}{\Delta y}(1-\theta)*\left(\eta^n_{i,j+1}-\eta^n_{i,j}\right)\right] \\
+\Delta t\tau^w_y \\
\Delta z_{M-1}\left[Fv^n_{i,j+\frac{1}{2},M-1}-g\frac{\Delta t}{\Delta y}(1-\theta)*\left(\eta^n_{i,j+1}-\eta^n_{i,j}\right)\right] \\
\vdots \\
\Delta z_{m+1}\left[Fv^n_{i,j+\frac{1}{2},m+1}-g\frac{\Delta t}{\Delta y}(1-\theta)*\left(\eta^n_{i,j+1}-\eta^n_{i,j}\right)\right] \\
\Delta z_m\left[Fv^n_{i,j+\frac{1}{2},m}-g\frac{\Delta t}{\Delta y}(1-\theta)*\left(\eta^n_{i,j+1}-\eta^n_{i,j}\right)\right]
\end{pmatrix} \tag{28}
$$

$$A=\begin{pmatrix} \Delta Z_M+a_{M-\frac{1}{2}} & -a_{M-\frac{1}{2}} & & 0 \\ -a_{M-\frac{1}{2}} & \Delta Z_{M-1}+a_{M-\frac{1}{2}}+a_{M-\frac{3}{2}} & -a_{M-\frac{3}{2}} & \\ & \ddots & \ddots & \ddots \\ 0 & & -a_{m+\frac{1}{2}} & \Delta Z_m+a_{m+\frac{1}{2}}+\gamma\Delta t \end{pmatrix} \tag{29}$$

where $a_k=\dfrac{\nu_k\Delta t}{\Delta z_k}$.

$$\Delta Z=\begin{pmatrix} \Delta z_M \\ \Delta z_{M-1} \\ \vdots \\ \Delta z_{m+1} \\ \Delta z_m \end{pmatrix} \tag{30}$$

$$\begin{aligned}\delta_{i,j}^n=\eta_{i,j}^n-&\frac{\Delta t}{\Delta x}(1-\theta)*\\ &\left[\left(\Delta Z_{i-\frac{1}{2},j}\right)^T U^n_{i+\frac{1}{2},j}-\left(\Delta Z_{i-\frac{1}{2},j}\right)^T U^n_{i-\frac{1}{2},j}\right]\\ -&\frac{\Delta t}{\Delta y}(1-\theta)*\left[\left(\Delta Z_{i,j+\frac{1}{2}}\right)^T V^n_{i,j-\frac{1}{2}}-\left(\Delta Z_{i,j-\frac{1}{2}}\right)^T V^n_{i,j-\frac{1}{2}}\right]\end{aligned} \tag{31}$$

Next, the expressions for U and V from Equations (18) and (19) are substituted into Equation (20), yielding

$$\begin{aligned}&\eta_{i,j}^{n+1}-g\frac{\Delta t^2}{\Delta x^2}\theta^2\left[\left[(\Delta Z)^T A^{-1}\Delta Z\right]^n_{i+\frac{1}{2},j}\left(\eta_{i+1,j}^{n+1}-\eta_{i,j}^{n+1}\right)\right.\\ &\qquad\left.-\left[(\Delta Z)^T A^{-1}\Delta Z\right]^n_{i-\frac{1}{2},j}\left(\eta_{i,j}^{n+1}-\eta_{i-1,j}^{n+1}\right)\right]\\ &-g\frac{\Delta t^2}{\Delta y^2}\theta^2\left[\left[(\Delta Z)^T A^{-1}\Delta Z\right]^n_{i,j+\frac{1}{2}}\left(\eta_{i,j+1}^{n+1}-\eta_{i,j}^{n+1}\right)\right.\\ &\qquad\left.-\left[(\Delta Z)^T A^{-1}\Delta Z\right]^n_{i,j-\frac{1}{2}}\left(\eta_{i,j}^{n+1}-\eta_{i,j-1}^{n+1}\right)\right]\\ &=\delta_{i,j}^n-\frac{\Delta t}{\Delta x}\theta\left[\left[(\Delta Z)^T A^{-1}G\right]^n_{i+\frac{1}{2},j}-\left[(\Delta Z)^T A^{-1}G\right]^n_{i-\frac{1}{2},j}\right]\\ &-\frac{\Delta t}{\Delta y}\theta\left[\left[(\Delta Z)^T A^{-1}G\right]^n_{i,j+\frac{1}{2}}-\left[(\Delta Z)^T A^{-1}G\right]^n_{i,j-\frac{1}{2}}\right]\end{aligned} \tag{32}$$

In this equation, A and A^{-1} are both positive definite matrices. Therefore $(\Delta Z)A^{-1}\Delta Z$ is non-negative number and Equation (32) constitutes a linear five-diagonal system of N_xN_y equations for η^{n+1}. This system is symmetric and positive definite. Thus, it has a unique solution that can be efficiently determined using the conjugate gradient method.

It is important to note that when the value of θ is 0.5, system (32) is well conditioned and the conjugate gradient method is able to achieve convergence even fast.

Once the free surface location for the next time step has been determined, Equations (18) and (19) constitute a set of simple $2N_xN_y$ linear tridiagonal systems for each *j*. These matrices are independent from each other, symmetric and positive definite. Therefore, they can be conveniently solved by a direct method.

The vertical velocity component *w* at the new time step can be computed by discretizing the continuity equation, Equation (3).

2.6 Numerical Stability

The stability analysis of the semi-implicit finite difference method is conducted using the von Neuman method. It is assumed that the governing differential equations are linear, have constant coefficients, and are across an infinite horizontal domain or with periodic boundary conditions in a finite domain[6].

This semi-implicit finite difference scheme is stable according to the von Neuman method if $1/2\leqq\theta\leqq 1$ and if the time step Δt satisfies the following inequality.

$$\Delta t\leq\left[2\mu_{II}\left(\frac{1}{\Delta x^2}+\frac{1}{\Delta y^2}\right)\right]^{-1} \tag{33}$$

The highest accuracy and efficiency is achieved when θ equals to 0.5. It should be noted that the stability of the semi-implicit finite difference scheme is independent of the velocity, bottom friction and vertical viscosity. It just depends on the horizontal viscosity. This method becomes unconditionally stable when the horizontal viscosity terms are neglected.

2.7 Overall Characteristics of the Numerical Model

Fig. 2 demonstrates the computational process. In this model, the surface elevation gradient in the momentum equations and the velocities in the free surface equation are discretized by the θ-method, with θ acting as a measure of implicitness, and the vertical mixing terms are discretized implicitly. The accuracy of the model is increased by adopting the Euler-Lagrangian method for discretizaing the convective and viscous terms instead of

the upwind scheme.

The CFL stability condition is not required by this method, because the barotropic pressure gradient in the momentum equations and the velocities in the vertical integrated continuity equation are implicitly formulated, resulting in the high efficiency of the model.

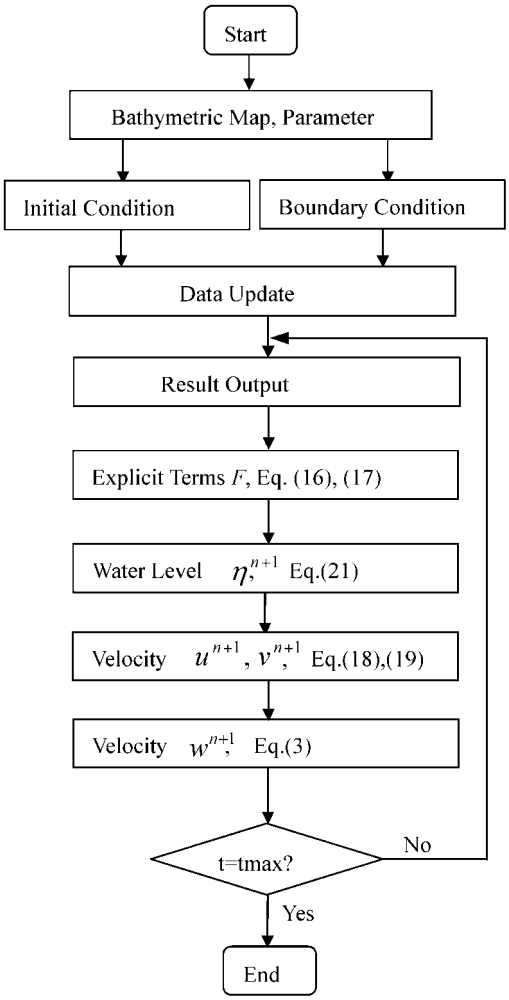

Fig. 2 Flow chart for numerical computations

3. Numerical Experiment for Simple Rectangular Basin

Before this three-dimensional tidal model is applied to an actual field, its accuracy and efficiency are verified through a simple application. A model bay of a rectangular shape with a constant depth as shown in Fig. 3 is subject to the tidal motion imposed at the open boundary with an amplitude of 0.5 m. The water depth is 10 m, the length and the width of the bay is 3.4 km and 1.5 km respectively. (The geometry and the horizontal mesh are shown in Fig. 3.) The analytical solution for this flow situation consists of the following equations (Ipppen, 1966)[7]:

$$\bar{u}(x,t) = \frac{A\varpi x}{h}\sin(\varpi t),\quad \eta = A\cos(\varpi t) \qquad (34)$$

In Equation (34), A is the wave amplitude; ϖ is the angular frequency ($2\pi/T$); h is the water depth; x is the distance from the left boundary; T is tidal period; $\bar{u}$ is the depth-averaged velocity component in the x-direction.

In the numerical computation, the water body is divided into 3 equal layers vertically. The other parameters are assigned as follows: $\Delta x = \Delta y = 100m$; $\Delta t = 60s$; $\mu_H = 0.0$; $\mu_V = 0.01m^2/s$; $T = 12hr$.

Fig. 4 shows a comparison between the numerical and analytical results of the free surface water elevation and the depth-averaged velocities. As can be seen in the figure, the analytical and numerical values are almost identical. A comparison of the numerical and analytical results reveal that the maximum water surface elevation agrees within 0.6%, and the maximum u-velocity components agree within 1.7%. Therefore,

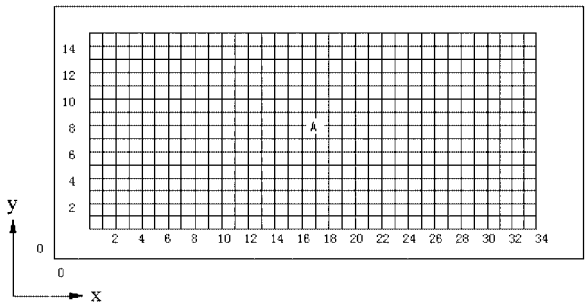

Fig. 3 Horizontal mesh used for the simulation of tide-induced circulation

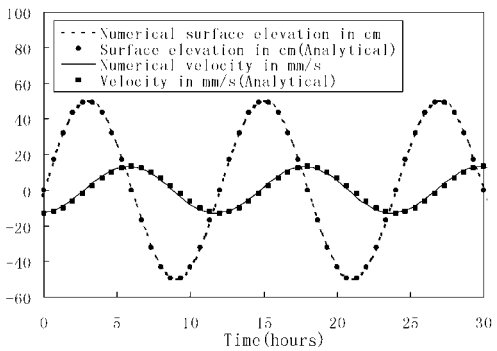

Fig. 4 Comparison of analytical and computed surface elevation and depth-averaged u-velocity profiles at A

this numerical experiment validates the accuracy and high efficiency of the proposed model. The numerical calculation was performed by a Pentium 4, 2.53 GHz PC. It only cost 10.770 CPU seconds to calculate 60×10000 seconds of real time for $35\times17\times3$ grids. The biggest time step allowed by the simulation program is 12 minutes.

4. Model Application to Dalian Bay

4.1 The Computational Region

The 3-D tidal model introduced above is next applied to Dalian Bay. Dalian Bay is located at the northern end of the Yellow Sea, as shown in Fig. 5. The bay is roughly rectangular, measuring approximately 10km wide and 10km long. As the economic development and the population have increased in the area, the pollution problems have become serious. More and more people are paying close attention to the environmental problems in China's coastal regions. Therefore, it is necessary to use the numerical model to study the hydrodynamic characteristics of this region.

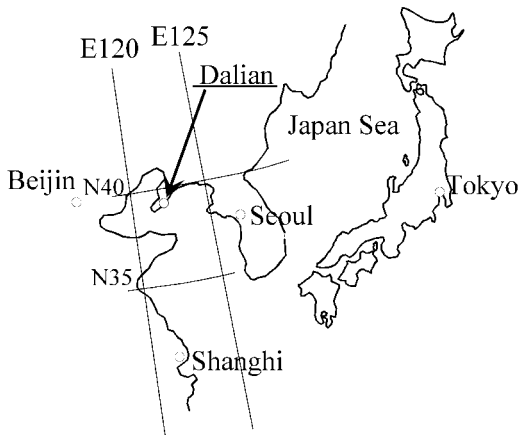

Fig. 5 The location of Dalian Bay

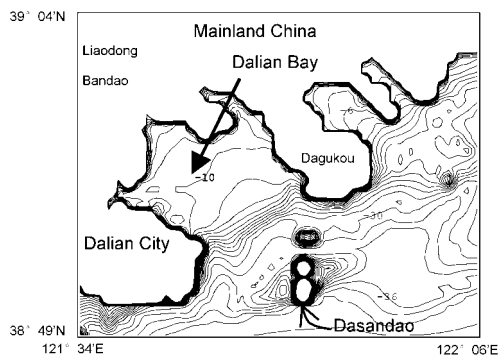

Fig. 6 Computational region of Dalian Bay

For this application, a computational measuring 32 km by 40 km is selected. Dalian Bay is situated in the center of the region, as shown in Fig. 6. The east and west boundaries are at the longitudes 121°34' E and 122°06' E respectively and the south and north boundaries are at the latitudes 38° 49' N and 39°04' N respectively. In the computational domain, the water depth ranges from about 1 m to 40 m. The area is divided into 32×40 grids with the spacing of 1000 m in the horizontal direction. The depth was divided into 14 numerical layers with the spacing of 3 m.

4.2 Tide-induced Currents

The tide-induced currents are essential factor in the transport phenomena of the coastal area, so the numerical accuracy of the results should be checked by the observed data. The main tide propagates from the southern region of the Yellow Sea. The dominant tidal components in this area are M_2 and S_2 tides. Therefore, the calculated tide in this study has a period of 12 hours, an amplitude of the sum of M_2 and S_2, and a phase lag of M_2 component. The validity of the numerical model is verified by checking the difference of the tidal harmonic components between the observed data and the numerical results. The model verification is carried out based on the tidal harmonic constants observed at the surrounding tidal stations. The tidal elevations in the domain are predicted by the model and the parameter values selected for the model verification are: $\Delta t = 60s$; $\mu_H = 1.0E\text{-}5 m^2/s$; $\mu_V = 1.0E\text{-}4 m^2/s$. The simulation run takes only 37.510 CPU seconds using a Pentium 4, 2.53 GHz PC. This simulation predicts the tidal currents after 84 hours' simulation.

The computed tidal elevations are shown in Figs. 7 and 8. It is evident from these figures that the computed and measured free surface water elevation coincide well at the selected stations. Because there is no flow field data for Dalian bay, no further comparison work can be performed.

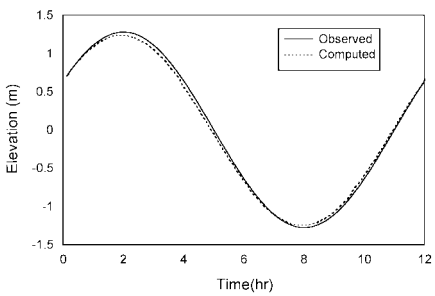

Fig. 7 Tide elevation at Dalian

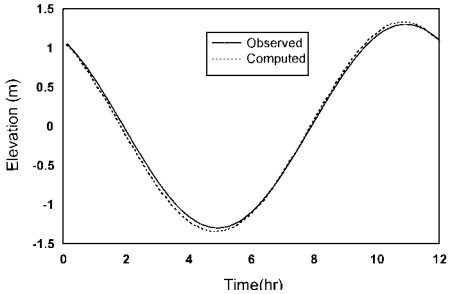

Fig. 8 Tide elevation at Dagukou

Figs. 9 (a) through 9 (d) show the surface flow vector fields in the Dalian Bay region for flood tide, high water level, ebb tide and low water level respectively.

From the vector field figures, the following conclusion can be made:

(1) In the eastern open sea region, the main direction of the tidal current is NE-SW. At the flood tide, the tidal current direction is SW and at the ebb tide, the tidal current direction is NE. In the eastern near-shore region, due to the effects of the bathymetry, the direction of the tidal current shows wide variability. In the region, the tidal direction acts parallel to the coastline. Also, there is an obvious revolving flow around the Dasan Island near the mouth of the bay. When the area is considered as a whole, the tidal current can be characterized as a reversing current.

(2) The velocities in the open sea are distributed evenly, with a maximum velocity of about 50 cm/s. The velocity decreases from the bay mouth region to the inside of the bay. The velocity is approximately 25 cm/s near the mouth of Dalian Bay, and is less than 5 cm/s near the inside the Bay.

(3) At the flood tide, the seawater flows into the bay from the east portion of the bay mouth and flows out from the west. The flow in reversed at the ebb tide. Due to the bathymetry effects and the incident tidal wave from the Yellow Sea, tidal flow circulation occurs inside the bay mouth. The bay's velocity distribution reveals that the velocity is higher and the water is easier to be exchanged with the open sea. For the region near the top of the bay, however, the velocity is lower and the water is difficult to be exchanged. The situation is not suitable for the pollutant to be washed out to the open sea.

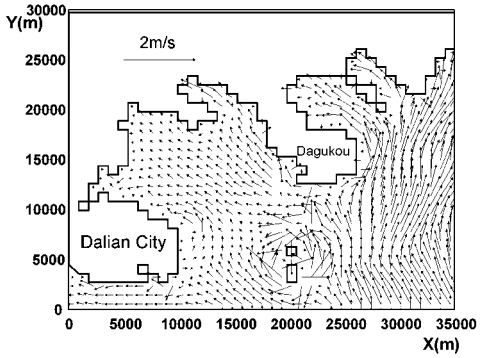

Fig. 9 (a) Velocity field for flooding tide

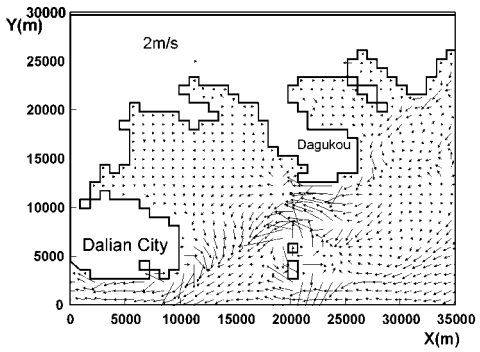

Fig. 9 (b) Velocity field for high water level

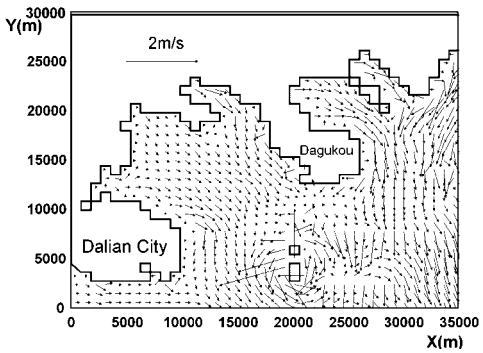

Fig. 9 (c) Velocity field for ebb tide

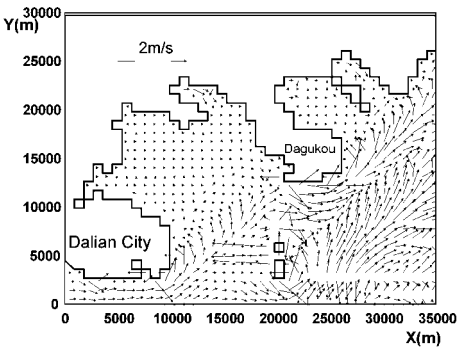

Fig. 9 (d) Velocity field for low water level

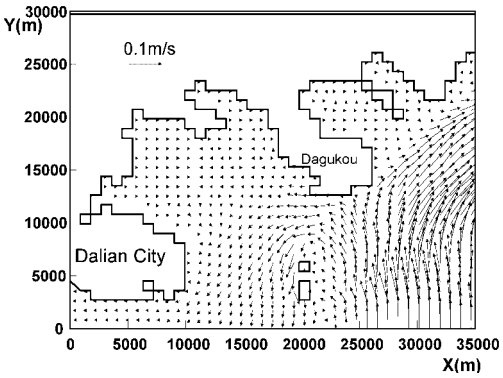

Fig.10 Tidal residual flow vectors

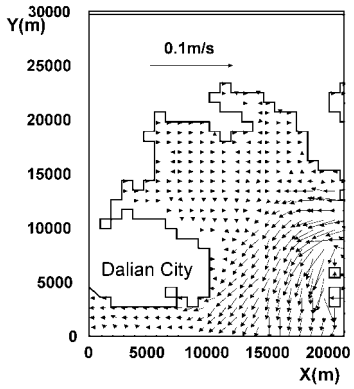

Fig. 11 Detailed Tidal residual flow vectors at Dalian Bay

Fig.10 shows the vertically averaged tidal residual current vectors. In this figure, the vertically averaging tidal residual currents are carried out for the all fourteen computational layers of computation. In the Yellow Sea side of the calculation domain, very strong clockwise current is observed. The results agree with the clockwise circulation of the Yellow Sea reported by Yanagi et al.[8]. Near the islands, however, some of the currents change to the clockwise direction.

In order to focus the study of the tidal residual currents on Dalian bay itself, an enlarged image of the flow vectors in this region is shown in Fig.11. It appears that the counterclockwise current at the mouth of the bay dose not affect currents within the bay.

Fig. 6 reveals that the bathymetry effects at the mouth of the bay have steep slope. The effect appears to prevent a large-scale circulation from entering Dalian Bay.

The depth of Dalian Bay can be as shallow as 10 m. Wind stress effects, which are not considered in this study, should act as a dominant factor in the hydraulic phenomena there. Adding the wind shear effect into the numerical model is straightforward, so it should be included in the future models. Seasonal wind data will be essential for this improved model.

6. Conclusions

An accurate and highly efficient three-dimensional tidal model has been introduced, and its applications have been discussed. At each time step the numerical method requires solving a large linear system that can be formally decomposed into a set of small three-diagonal systems coupled with one five-diagonal system. Because this model does not require the CFL stability condition, a high efficiency can be realized. The accuracy of the model is ensured through the use of Euler-Lagrangian method to discretize the convective and viscous terms. Both the numerical results and the computational speed for the numerical experiment and the application of Dalian Bay verify the accuracy and high efficiency of the model. The Dalian Bay simulation reveals that the side-to-side reversing current is dominant in the bay and the current speed decreases from the bay mouth to the inside of the bay.

The current performance of numerical scheme is quite satisfactory. In the future, the effects of wind stress, density driven currents generated by seasonal atmospheric temperature change will be included in the numerical calculation. Applying the model to ecological problems can be an example of extension of the model because the problems caused by difference of time scale between ecological and dynamic phenomena will be overcome by highly efficient scheme proposed in this study.

REFERENCE

1) Kim, C. and Lee, J.: A three-dimensional PC-based hydrodynamic model using an ADI scheme, *Coastal Engineering*, Vol.23, pp.271-287, 1994.

2) Abbott, M. B.: Range of tidal flow modeling, *Journal of Hydraulic Engineering*, ASCE, Vol.123, pp.257-277, 1997.

3) Davis, A. M., Jones, J.E. and Xing, J.: Review of recent developments in tidal hydrodynamic modeling. I: special models, *Journal of Hydraulic Engineering*, ASCE, Vol.123, pp.278-292, 1997.

4) Weare, T. J.: Errors arising from irregular boundaries in ADI solutions of the shallow-water equations, *International Journal for Numerical Methods in Engineering*, Vol.14, pp.921-931, 1979.

5) Casulli, V.: Semi-implicit finite difference methods for three-dimensional shallow water flow, *International Journal for Numerical Methods in Fluids*, Vo.15, pp.629-648, 1992.

6）Casulli, V. and Catani, E.: Stability, accuracy and efficiency of a semi-implicit method for three-dimensional shallow water flow, *Computers & Mathematics with Application*, Vol. 27（4）, pp.99-112, 1994.
7）Ippen, A.T.: Estuary and coastal hydrodynamics. McGraw Hill, New York, 1966.
8）Yanagi, T. and Takahashi, S.: Seasonal variation of circulation in the east China Sea and the Yellow Sea, *Journal of Oceanography*, Vol.49, pp.503-520, 1993.